Front. Struct. Civ. Eng. 2021, 15(2): 412–424
https://doi.org/10.1007/s11709-021-0700-5

RESEARCH ARTICLE

Crushed rocks stabilized with organosilane and lignosulfonate in pavement unbound layers: Repeated load triaxial tests

Diego Maria BARBIERI[a*], Inge HOFF[a], Chun-Hsing HO[b]

[a] *Department of Civil and Environmental Engineering, Norwegian University of Science and Technology, Trondheim, Trøndelag 7491, Norway*

[b] *Department of Civil and Environmental Engineering, Northern Arizona University, Flagstaff, AZ 86011, USA*

[*] *Corresponding author. E-mail: diego.barbieri@ntnu.no*

ABSTRACT The creation of the new "Ferry-Free Coastal Highway Route E39" in southwest Norway entails the production of a remarkable quantity of crushed rocks. These resources could be beneficially employed as aggregates in the unbound courses of the highway itself or other road pavements present nearby. Two innovative stabilizing agents, organosilane and lignosulfonate, can significantly enhance the key properties, namely, resilient modulus and resistance against permanent deformation, of the aggregates that are excessively weak in their natural state. The beneficial effect offered by the additives was thoroughly evaluated by performing repeated load triaxial tests. The study adopted the most common numerical models to describe these two key mechanical properties. The increase in the resilient modulus and reduction in the accumulated vertical permanent deformation show the beneficial impact of the additives. Furthermore, a finite element model was created to simulate the repeated load triaxial test by implementing nonlinear elastic and plastic constitutive relationships.

KEYWORDS organosilane, lignosulfonate, crushed rocks, pavement unbound layers, repeated load triaxial test, finite element analysis

1 Introduction

1.1 Project background

According to the Norwegian Public Roads Administration (NPRA), the overarching aim of the "Ferry-Free Coastal Highway Route E39" project is to enhance the condition of the existing road network along the coast of southwest Norway by revamping the highway infrastructure present between Trondheim and Kristiansand [1]. This project is highly significant for the Norwegian economic system [2]. The widespread tunneling blasting operations that are being conducted to create new and faster routes generate considerable quantities of crushed rocks. These resources could be employed as aggregates in the unbound courses of the highway itself or other road pavements present nearby, thus curtailing the use of non-local materials, promoting a sustainable construction [3–5], and consequently bolstering Norway's national goal of becoming carbon neutral during this decade [6].

To avoid the formation of excessive distresses in the road structure [7], the NPRA demands that the aggregates (unbound granular materials, UGMs) meet some qualification tests [8,9] regarding shape [10], flakiness [11], resistance to fragmentation (Los Angeles test, LA) [12], and resistance to wear (micro-Deval test, MDE) [13,14].

Previous research [15] has investigated the geological origin of rocks present along the E39 highway. Three rock types (referred to as M1, M2, and M3) were collected and characterized according to the aforementioned standard tests. The qualification tests are met by M1 ("strong" aggregates), whereas M2 and M3 exceed the limit values of the LA and MDE tests ("weak" aggregates) and

Article history: Received Jul 12, 2019; Accepted Apr 9, 2020

therefore cannot be employed in their natural status in the unbound courses of road pavements.

1.2 Stabilization technologies

In recent decades, different stabilization solutions for unbound materials have been investigated, e.g., bitumen, cement, fly ash, and lime, just to mention a few [16–23]. Furthermore, two innovative technologies have exhibited preliminary positive outcomes when it comes to enhancing the mechanical properties of "weak" aggregates [24]. These stabilizing agents are based on organosilane and lignosulfonate, and are designated as polymer-based (P) additive and lignin-based (L) additive in this study, respectively. These technologies modify the mechanical performance of aggregates entailing macroscopic enhancement [25–29]. The P agent promotes the creation of strong siloxane (= Si-O-Si =) chemical polar bonds. The L agent is an organic product comprising both hydrophilic and hydrophobic linkages [30,31].

1.3 Objectives

The effectiveness of the stabilizing agents was investigated in the laboratory by means of repeated load triaxial tests (RLTTs), which evaluated the resilient modulus and resistance against permanent deformation. The most common numerical models were adopted to describe these two key mechanical properties, thus expanding the research accomplished thus far [32].

Furthermore, a finite element model simulating the RLTT was created. Numerical analyses were carried out to study the behavior of UGMs, and non-linear elastic and plastic constitutive relationships were considered [33]. The experimental and numerical results were compared in terms of vertical permanent deformation.

2 Materials and methods

2.1 Materials tested

Referring to the three crushed rock types (M1, M2, and M3) initially collected [15] to represent the geology spread along the highway alignment, this study focuses on the weak material M2. It has a metamorphic origin and is a fine-grained felsic and micaceous rock. The numerical models adopted and discussed for M2 in the following sections could also be analogously extended to M3 (or other aggregate types).

2.2 Repeated load triaxial test

The stiffness and the resistance to permanent deformation of UGMs were thoroughly investigated using RLTTs. The stress level, moisture content, dry density, grading, and mineralogy [34–37] are the most relevant variables that determine the mechanical performance.

Figure 1 displays the preparation procedure for running a RLTT. Initially, 7300 g of aggregates were blended (Fig. 1(a)) considering the selected gradation depicted in Fig. 2 with the reported upper and lower grain size distribution curves for a base layer [7,8]. Water and additive, if necessary, are added to the aggregates, which rest for 24 h to allow the moisture to be distributed uniformly inside plastic bags (Fig. 1(b)). Both organosilane and lignosulfonate were blended with M2 at the optimum moisture content (OMC), which is equal to 5% in mass for the considered grading curve distribution. The quantity of organosilane mixed with the crushed rocks was 0.5% (40 g), and the amount of lignosulfonate added was 1.5% (120 g). The former admixture is effective after application, whereas the latter admixture requires curing to attach to the aggregates. A Kango 950X vibratory hammer (total weight 35 kg, frequency 25–60 Hz, amplitude 5 mm) compacted the specimen layers for 30 s (Fig. 1(c)); the bulk density and dry density were assessed as specified by Ref. [38]. The sample was fully compacted inside the steel mold (Fig. 1(d)); afterwards, it was extracted vertically by means of a dedicated ejecting tool and the specimen was encapsulated in a latex membrane (Fig. 1(e)). In the last step, another latex membrane, two metal end plates, four plastic rings, and two hose clamps sealed the sample, thus avoiding the penetration of the water used to exert the confining pressure (Fig. 1(f)). Three and three linear variable differential transducers (LVDTs) evaluated the axial and radial deformations, respectively (Fig. 1(g)). Finally, the test was ready to run (Fig. 1(h)).

Two types of stresses were applied during the RLTT: uniform confining stress (σ_t, triaxial or confining) and vertical dynamic stress (σ_d, deviatoric); the latter varied following a sinusoidal pattern. According to the multi-stage low stress level (MS LSL) testing procedure, five σ_t values (σ_t = 20, 45, 70, 100, and 150 kPa) defined as many testing sequences: each sequence comprised six steps and each step was characterized by a precise σ_d peak value [39]. Figure 3 reports the stress path for the MS LSL procedure considering σ_d and the bulk stress θ ($\theta = \sigma_1 + \sigma_2 + \sigma_3 = \sigma_d + 3\sigma_t$, where σ_1, σ_2, σ_3 are the principal stresses). One RLTT included up to 30 loading steps; for each of them, the peak value of σ_d was applied 10000 times with a frequency of 10 Hz. The overall results were assessed by testing two replicate specimens for each studied proportioning. For example, Figure 4 shows three investigated samples after completion of the RLTT.

As previously mentioned, the L additive requires curing to attach to the material particles. Therefore, the samples (Figure 1(f)) treated with this agent were conditioned at 50°C for 24 h and subsequently at 22°C for 24 h, reaching a water content of approximately 2%. Their performance was compared to that of untreated samples with water content w = 1% in mass. This is a conservative evaluation

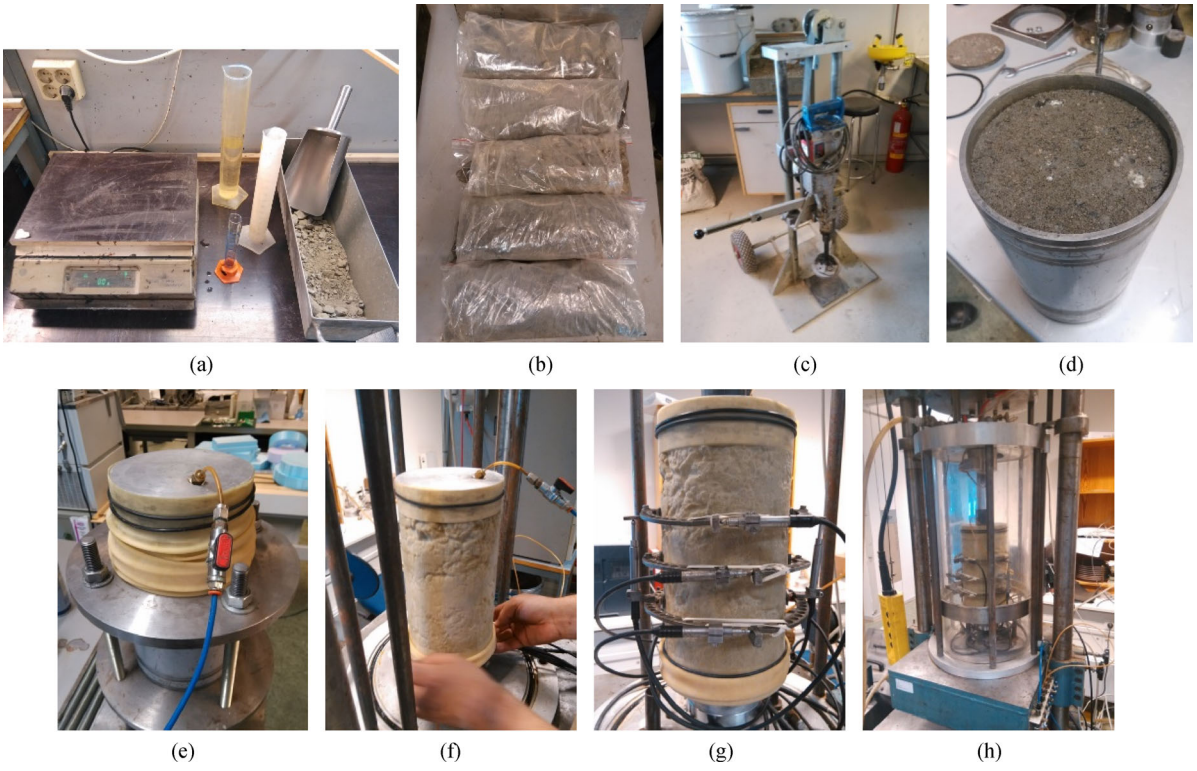

Fig. 1 RLTT specimen preparation phases. (a) Preparation of the aggregates; (b) aggregates mixed with water/additive; (c) hammer for specimen compaction; (d) mold with compacted specimen; (e) extraction of the specimen from the mold; (f) placement of the specimen inside the triaxial chamber; (g) mounting of LVDTs on the specimen; (h) specimen ready for triaxial testing.

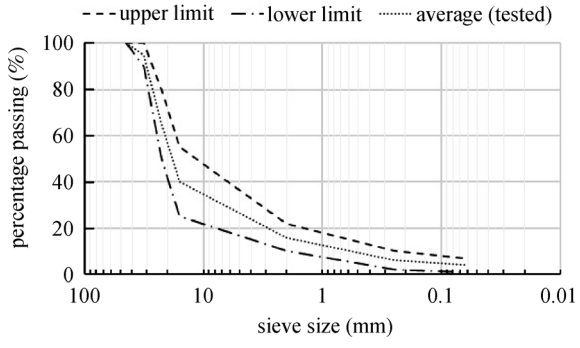

Fig. 2 Grading curves for road base layer.

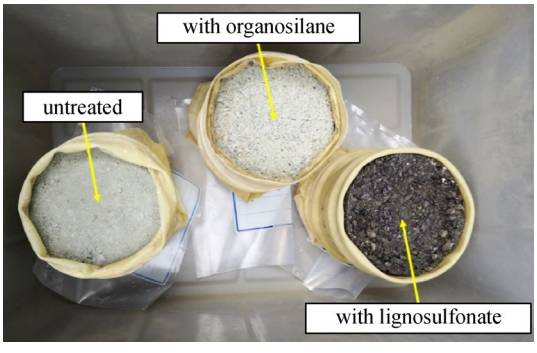

Fig. 4 Three illustrative RLTT samples: untreated, with organosilane, with lignosulfonate.

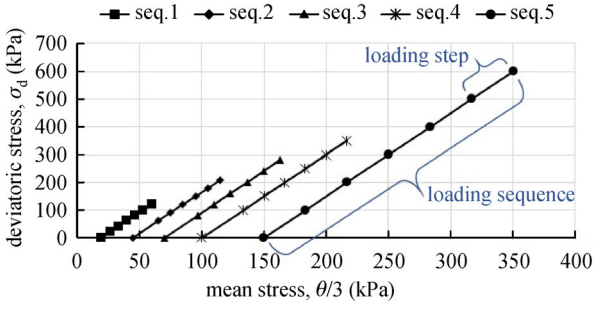

Fig. 3 Loading sequences and steps for the MS LSL procedure.

as the mechanical properties reduce when w augments [40]. In contrast, the P additive is effective after its application; therefore, these treated samples were compared to untreated samples with w = 5%. Because of the differences in w, the results described in Sections 3.1 and 3.2 are portrayed with two plots each time: one referring to organosilane, and one referring to lignosulfonate.

2.3 Resilient modulus

Given a dynamic deviatoric stress $\Delta\sigma_d$ and a constant σ_t, the resilient modulus M_R is expressed as

$$M_R = \frac{\Delta\sigma_d}{\varepsilon_{ve}}, \quad (1)$$

where ε_{ve} is the vertical resilient strain. The resilient modulus represents the UGM behavior under repeated traffic loading and is a key parameter for any mechanistically based design method [33,41,42].

M_R can be efficiently described by non-linear relationships considering a variety of different parameters [35]; the equations presented in the following subsections are used to evaluate the M_R of the RLTT samples. All regression parameters are obtained through the least-square method.

2.3.1 Hicks and Monismith model

Hicks and Monismith formulated a simple and effective connection between M_R and θ [43].

$$M_R = k_{1,HM}\sigma_a\left(\frac{\theta}{\sigma_a}\right)^{k_{2,HM}}, \quad (2)$$

where σ_a is the reference pressure (100 kPa) and $k_{1,HM}$, and $k_{2,HM}$ are regression parameters. This relationship proposes a neat evaluation of the mechanical performance in an M_R–θ plot. Owing to its simplicity, this model is mostly used to interpret the resilient modulus of UGMs [35].

2.3.2 Uzan model

The Uzan model considers the presence of three parameters, namely, M_R, θ, and σ, as in Ref. [44]

$$M_R = k_{1,UZ}\sigma_a\left(\frac{\theta}{\sigma_a}\right)^{k_{2,UZ}}\left(\frac{\sigma_d}{\sigma_a}\right)^{k_{3,UZ}}, \quad (3)$$

where $k_{1,UZ}$, $k_{2,UZ}$, and $k_{3,UZ}$ are regression parameters. In addition to the formulation proposed by the Hicks and Monismith model, the one suggested by Uzan considers the bulk stress and deviatoric stress at the same time. These two factors are the most important factors affecting the resilient modulus of UGMs [35]. The Uzan model enables a useful comparison in a three-dimensional M_R, θ, and σ_d plot. It is also worth mentioning the Uzan and Witczak model, which takes into consideration the octahedral shear stress τ_{oct} instead of the deviatoric stress σ_d in order to include full three-dimensional conditions [45]. Nevertheless, the application of the Uzan and Witczak model is of limited interest in this study, as τ_{oct} can be easily correlated to σ_d as follows: $\tau_{oct} = \sqrt{2}\sigma_d/3$, for $\sigma_2 = \sigma_3$ (condition valid for the performed RLTTs).

2.4 Accumulated permanent deformation

The deformational response of UGMs can be divided into two parts: elastic (or resilient) and plastic (or permanent). The latter, occurring due to the wearing and crushing of the grains, may lead to pavement distress (rutting, potholes, cracking, etc.) [36]. Moreover, the UGM permanent deformation consists of two phases. In the first phase, there is a rapid increase in permanent strain with the application of load; in the second phase, the deformation rate becomes constant and is characterized by volume change [46,47]. The permanent deformation increases with moisture content, as water reduces the effective stress and friction [40].

A number of formulations can be employed to describe the development of vertical permanent deformation ε_{vp} based on the applied load pulses N or as a combination of one or more of the following parameters: mean bulk stress θ_m ($\theta_m = \theta/3$), mean deviatoric stress $\sigma_{d,m}$ ($\sigma_{d,m} = \sigma_d/3$), and vertical resilient deformation ε_{ve} [48].

$$\varepsilon_{vp} = f_1(N)f_2(\theta_m,\sigma_{d,m},\varepsilon_{ve}). \quad (4)$$

This study takes into consideration the models described in the following subsections. All regression parameters are obtained through the least-square method. As illustrated in Section 2.2, an RLTT is composed of 30 steps (or, equivalently, 30 stress-paths); the data obtained for each step are fitted, which may create discontinuities between the end of a step and the beginning of the following one, as displayed in the images in Section 3.2.

2.4.1 Coulomb model

The Coulomb formulation considers that the mobilized angle of friction ρ and the angle of friction at incremental failure φ describe the degree of mobilized shear strength and the maximum shear strength, respectively [49]. Consequently, these two angles define the material according to three types of performance (elastic, elasto-plastic, and failure) as presented in Table 1, in which each loading step is classified based on the average strain rate $\dot{\varepsilon}$ developed between the cycles from 5000 to 10000 [49].

Table 1 Material classification based on the development of plastic deformation

$\dot{\varepsilon}$	performance
$\dot{\varepsilon} < 2.5 \times 10^{-8}$	elastic range
$2.5 \times 10^{-8} < \dot{\varepsilon} < 1.0 \times 10^{-7}$	elasto-plastic range
$\dot{\varepsilon} > 1.0 \times 10^{-7}$	failure range

The elastic limit and the failure limit are defined by the following equations, respectively:

$$\sigma_d = \frac{2\sin\rho(\sigma_3 + a)}{1 - \sin\rho}, \quad (5)$$

$$\sigma_d = \frac{2\sin\varphi(\sigma_3 + a)}{1 - \sin\varphi}, \quad (6)$$

where the apparent attraction a is specified as 20 kPa [37].

2.4.2 Barksdale model

Barksdale studied the UGM behavior by means of RLTTs and found that the accumulation of permanent vertical strain ε_{vp} is proportional to the logarithm of the number N of load cycles [50] as follows:

$$\varepsilon_{vp} = a_{BA} + b_{BA}\mathrm{Log}(N), \tag{7}$$

where a_{BA} and b_{BA} are regression parameters.

2.4.3 Sweere model

Sweere also performed a series of RLTTs on UGMs and found that the logarithm of permanent vertical strain ε_{vp} is proportional to the logarithm of the number N of load cycles [51] as follows:

$$\log(\varepsilon_{vp}) = a_{SW} + b_{SW}\mathrm{Log}(N), \tag{8}$$

where a_{SW} and b_{SW} are regression parameters.

2.4.4 Time hardening approach for Barksdale and Sweere models

Both the Barksdale and Sweere models have been developed to fit the data of a single-stage (SS) RLTT. The results are plotted in a graph with the number N of load repetitions along the x-axis and the accumulated vertical permanent deformation ε_{vp} along the y-axis, where the first value is equal to zero. In a multi-stage (MS) RLTT, the first ε_{vp} of each loading step is different from zero (except for the first RLTT step). As this study performs MS RLTTs, the time hardening approach is adopted to describe the experimental data [52,53]. According to the time hardening approach, the ε_{vp} values corresponding to each loading step are treated as the last part of as many curves; each of them ideally corresponds to an SS RLTT, in which the first ε_{vp} is zero. This study calculates 30 curves (one for each loading step). Each curve is evaluated using the least-square method with a third-order polynomial expression. The data used to evaluate this third-order polynomial curve are the experimental ε_{vp} values for the specific step. Finally, for each loading step, the parameters of the chosen model (a_{BA}, b_{BA} for the Barksdale model or a_{SW}, b_{SW} for the Sweere model) are calculated through a least-square regression considering the experimental ε_{vp} values of the specific loading step and the first point of the ideal curve (with the first ε_{vp} value equal to zero).

2.4.5 Hyde model

Hyde established the following formulation for permanent vertical strain ε_{vp} encompassing the mean deviatoric stress $\sigma_{d,m}$ and triaxial stress σ_t [54]:

$$\varepsilon_{vp} = a_{HY}\frac{\sigma_{d,m}}{\sigma_t}, \tag{9}$$

where a_{HY} is a regression parameter.

2.4.6 Shenton model

Shenton proposed the following formulation for permanent vertical strain ε_{vp} including the maximum mean deviatoric stress $\sigma_{d,m,max}$, and triaxial stress σ_t [55]:

$$\varepsilon_{vp} = a_{SH}\left(\frac{\sigma_{d,m,max}}{\sigma_t}\right)^{b_{SH}}, \tag{10}$$

where a_{SH} and b_{SH} are regression parameters.

2.5 Finite element method RLTT modeling

The RLTT is modeled using COMSOL Multiphysics software [56]. The goal is to describe the accumulation of vertical permanent deformation, and the numerical and experimental results are compared. Figure 5 shows a portion of the model; the problem is two-dimensional axisymmetric, and quadrilateral elements are used in the mesh (height 180 mm, radius 75 mm, Poisson's ratio 0.3, and density 2300 kg/m^3). A fixed boundary constraint was applied at the bottom.

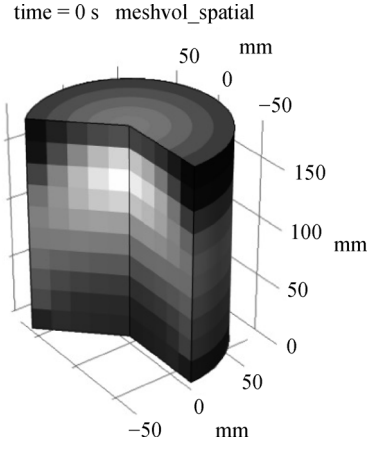

Fig. 5 Mesh of the finite element method RLTT model.

Different models can describe the UGM behavior: nonlinear elastic [33,57] and plastic [58,59] relationships have been used by researchers to interpret the UGM behavior. The following subsections detail the constitutive relationships implemented in this study.

A time-dependent analysis is performed and the total time is 30000 s, which is the actual duration of an RLTT. Each loading step, as reported in Section 2.2, corresponds to a specific combination of σ_t and σ_d and lasts for 1000 s; the repetition of the deviatoric pulse is not considered.

2.5.1 Modeling non-linear elasticity

COMSOL Multiphysics enables the implementation of a non-linear elastic model by specifying the elastic modulus law. The resilient moduli obtained by the Hicks and Monismith and Uzan models are implemented.

2.5.2 Modeling plasticity

Tresca and von Mises yield criteria are used to model the associated flow plasticity. Each model requires the definition of two parameters, the initial yield stress σ_y and plastic tangent modulus, to define the linear isotropic hardening. The initial yield stress σ_y is equal to the deviatoric stress σ_d of each loading step because plastic deformation takes place from the beginning of each step. The plastic tangent modulus is evaluated as a secant value using the least-squares method in a graph displaying $\sigma_1 - \sigma_3$ along the y-axis and ε_{vp} along the x-axis for the Tresca model or $(2/3)\cdot\varepsilon_{vp}$ along the x-axis for the von Mises model, as illustrated in Figs. 6 and 7, respectively.

Even if UGMs derive the bulk of their strength from friction, and the Tresca and von Mises criteria contain no frictional strength components, these models can represent the cohesion generated by the stabilizing additives.

Furthermore, UGMs are not regarded as viscous materials in the sense that applying a constant load does not cause a time-dependent deformation. It may be worth mentioning that models for viscosity could be adapted to account for the gradual increase in ε_{vp} per RLTT load cycle [60].

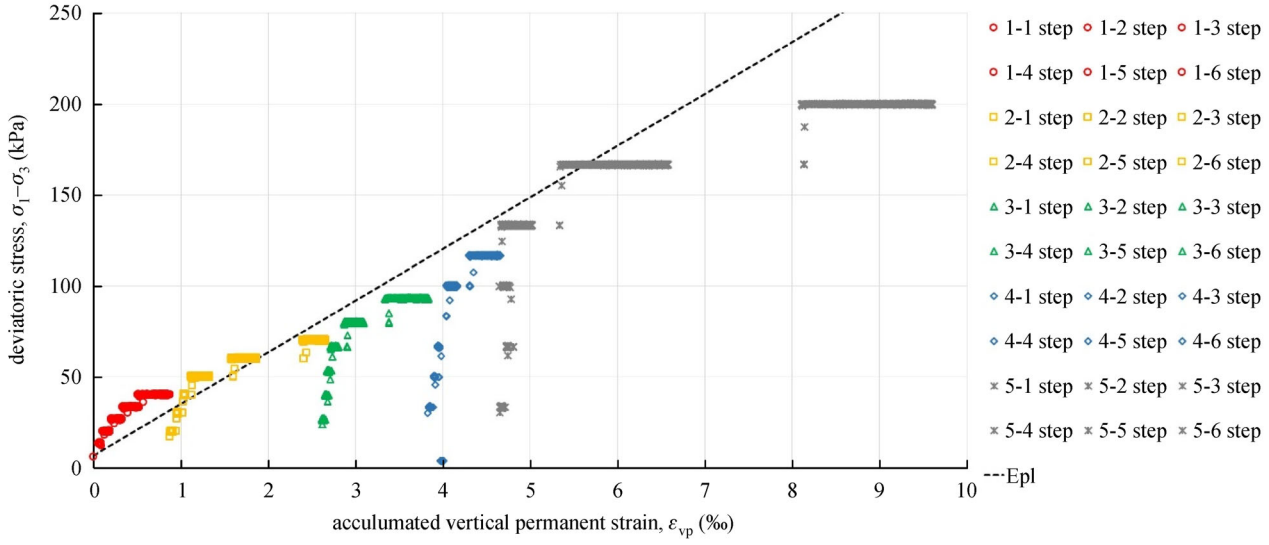

Fig. 6 Evaluation of Tresca plastic tangent modulus.

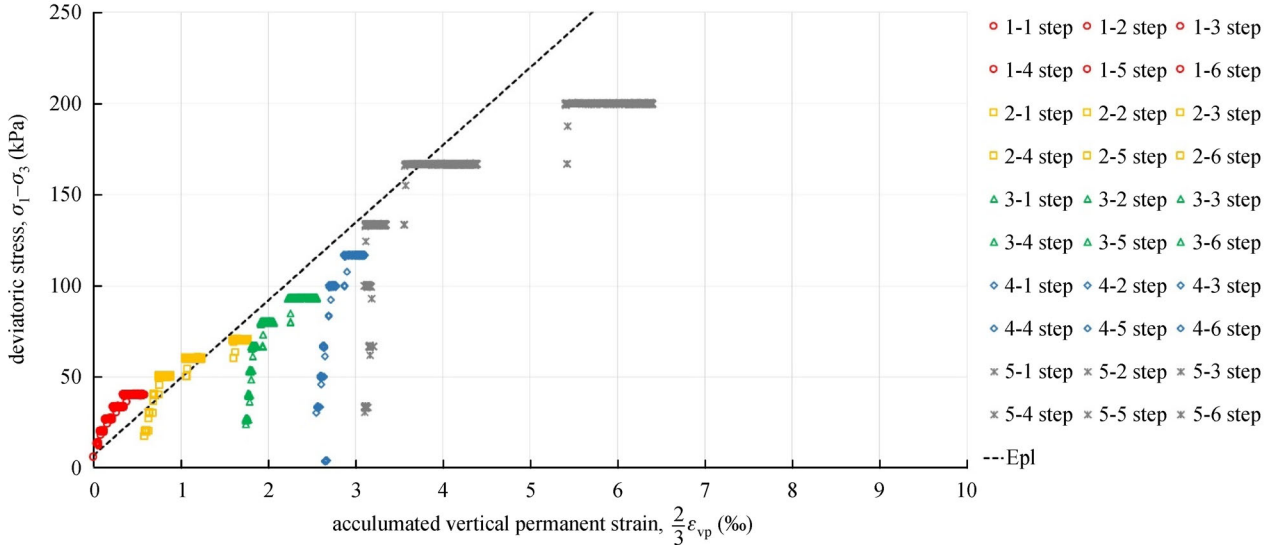

Fig. 7 Evaluation of Von Mises plastic tangent modulus.

3 Test results and discussion

3.1 Resilient modulus

Figures 8(a) and 8(b) display M_R based on the Hicks and Monismith formulation. The black and magenta colors correspond to untreated and treated materials, respectively.

In addition to the Hicks and Monismith model, the Uzan model takes into consideration the deviatoric stress σ_d as a further parameter to characterize M_R. The three-dimensional plots reported in Figs. 9(a) and 9(b) refer to P and L additives, respectively.

Table 2 presents the values of the regression parameters for the Hicks and Monismith and Uzan models.

All the models clearly show that the additives are effective solutions to enhance the resilient modulus M_R of the aggregates.

3.2 Accumulated permanent deformation

The use of the stabilizing technologies also leads to significative improvements when it comes to the deformation properties of the aggregates. Figure 10 shows the mobilized angle of friction ρ and the angle of

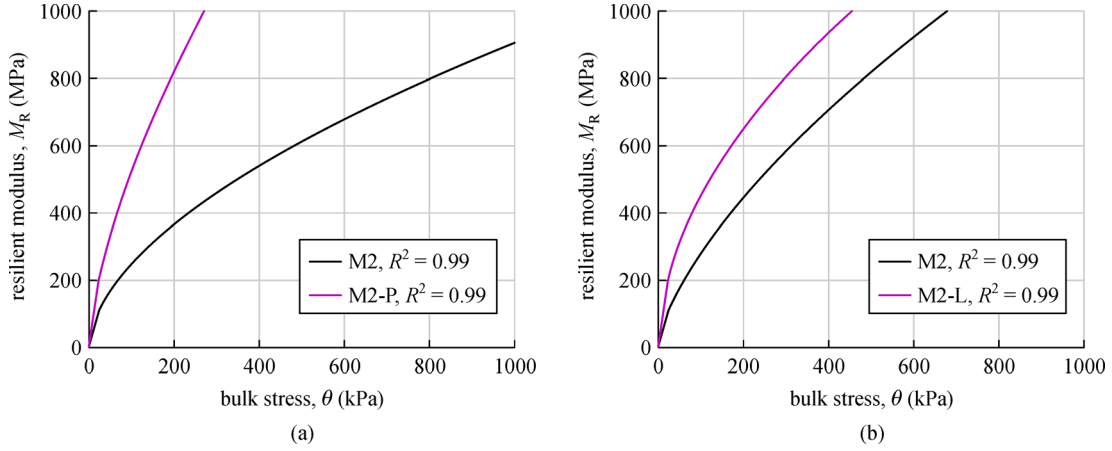

Fig. 8 Resilient modulus based on Hicks and Monismith formulation: (a) polymer-based (P) additive; (b) lignin-based (L) additive.

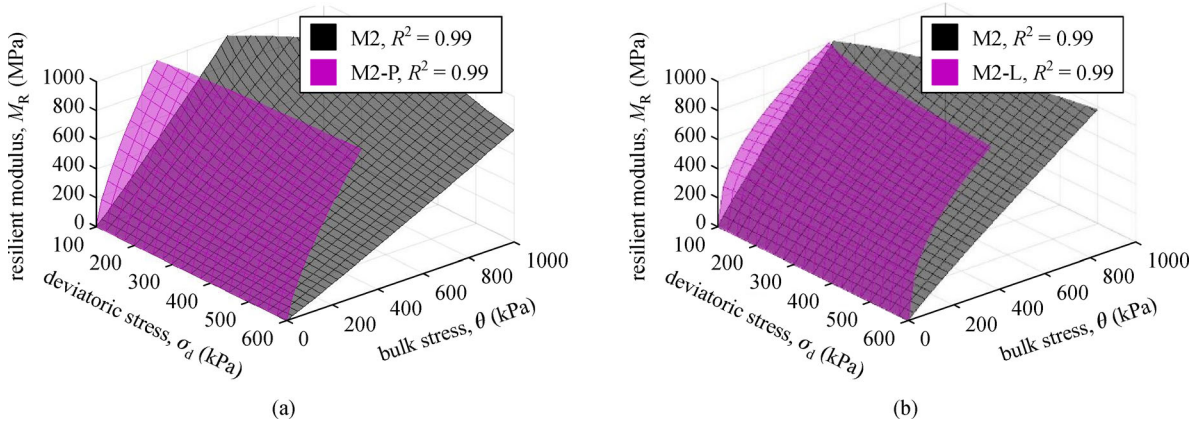

Fig. 9 Resilient modulus based on Uzan and Witczak formulation: (a) P additive; (b) L additive.

Table 2 Regression parameters for Hicks and Monismith, Uzan models

material	Hicks and Monismith		Uzan		
	$k_{1,HM}$	$k_{2,HM}$	$k_{1,UZ}$	$k_{2,UZ}$	$k_{3,UZ}$
M2 (w = 5%)	2467	0.56	1577	1.06	–0.47
M2-P	5206	0.65	4813	0.74	–0.08
M2 (w = 1%)	2860	0.66	2216	0.92	–0.25
M2-L	4530	0.52	4881	0.45	0.06

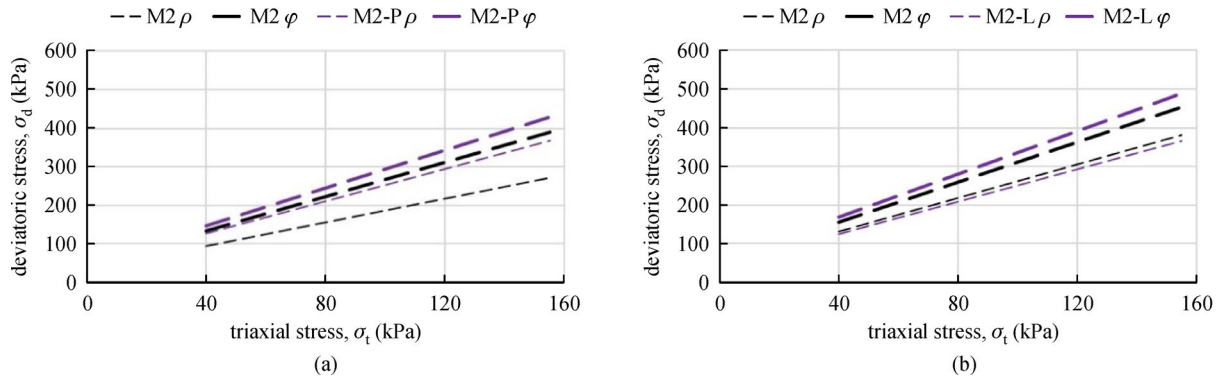

Fig. 10 Mobilized angle of friction ρ and angle of friction at incremental failure φ: (a) P additive; (b) L additive.

friction at incremental failure ϕ for the untreated and treated materials; both angles, ρ and ϕ, are enhanced by applying the additives. Table 3 details the values of the boundary angles.

Table 3 Values of limit angles ρ and φ

material	limit angles	
	ρ	φ
M2 (w = 5%)	57.2	65.8
M2-P	64.6	67.8
M2 (w = 1%)	65.4	68.9
M2-L	64.4	70.3

The accumulated vertical permanent deformations evaluated according to the Barksdale and Sweere models are shown in Figs. 11 and 12, respectively. These criteria fit the experimental data corresponding to each single loading step with the time hardening approach discussed in Subsection 2.4.4. The treated materials show considerably less permanent deformation than the untreated materials.

The Hyde model results are displayed in Figure 13. Each loading sequence corresponds to a straight line; therefore, five straight lines correspond to the MS RLTT.

Table 4 reports the regression parameter a_{HY} corresponding to each RLTT loading sequence.

The Shenton model results are displayed in Fig. 14. Each loading sequence corresponds to a curve; therefore, five curves correspond to the MS RLTT.

Table 5 reports the values of the regression parameters a_{SH} and b_{SH} for each loading sequence. All the models adopted to describe the accumulation of permanent deformation indicate that the treated aggregates perform better than the untreated ones.

3.3 Finite element method RLTT modeling

The aim of the modeling is to evaluate the permanent vertical deformations ε_{vp} and compare the numerical and experimental results. The choice of the nonlinear elastic model (Hicks and Monismith, Uzan) is irrelevant, as this part does not entail plastic deformations. The first modeling attempt implements the Tresca plasticity criterion. Figure 15(a) displays the results for the P additive, whereas Fig. 15(b) shows the results for the L additive.

The second modeling attempt implements the von Mises plasticity criterion. Figure 16(a) displays the results for the

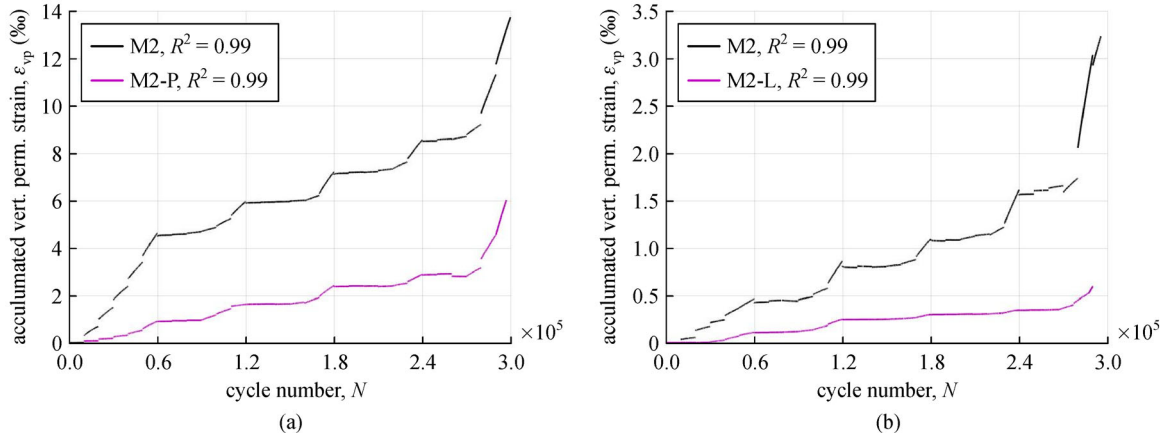

Fig. 11 Accumulated vertical permanent deformation, Barskdale model: (a) P additive; (b) L additive.

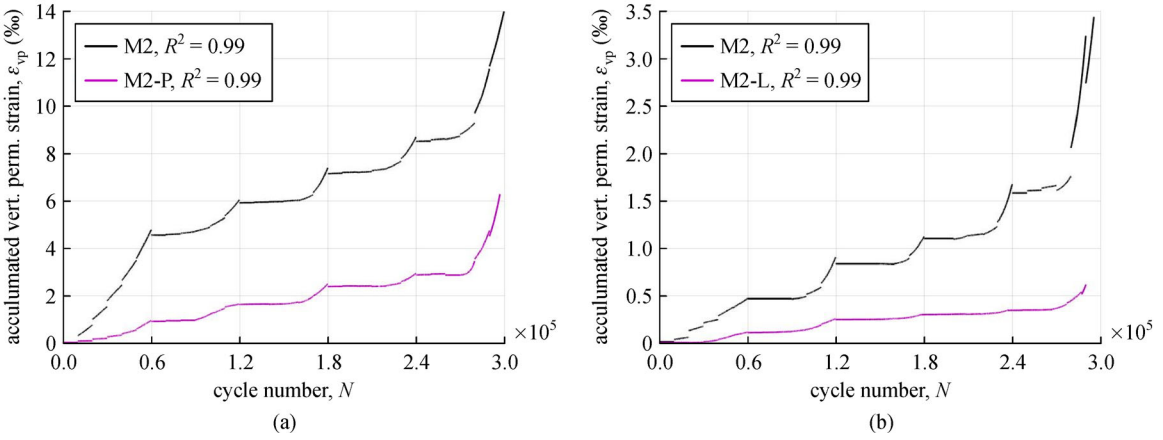

Fig. 12 Accumulated vertical permanent deformation, Sweere model: (a) P additive; (b) L additive.

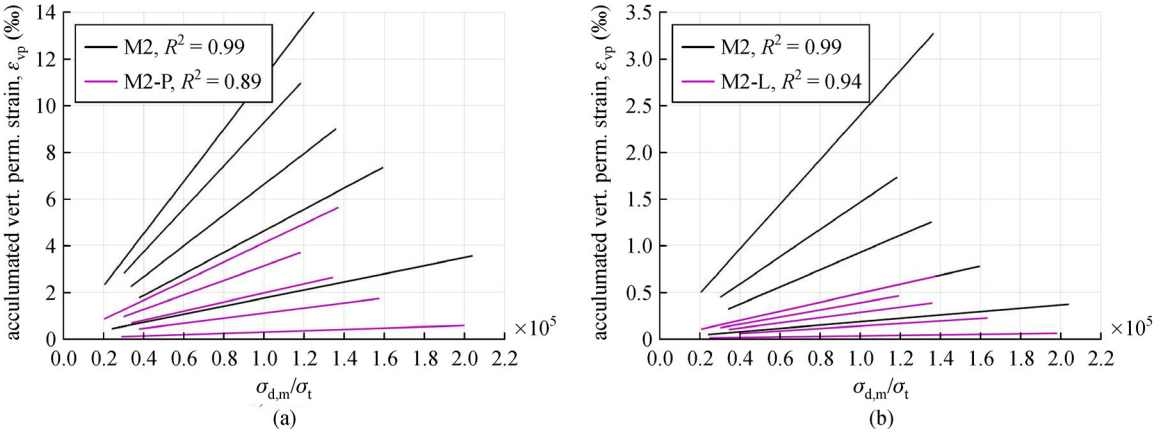

Fig. 13 Accumulated vertical permanent deformation, Hyde model: (a) P additive; (b) L additive.

Table 4 Values of a_{HY} for Hyde model

material	seq 1	seq 2	seq 3	seq 4	seq 5
M2 (w = 5%)	1.74	4.60	6.60	9.23	11.18
M2-P	0.28	1.09	1.96	3.12	4.09
M2 (w = 1%)	0.18	0.49	0.92	1.46	2.39
M2-L	0.03	0.13	0.28	0.38	0.49

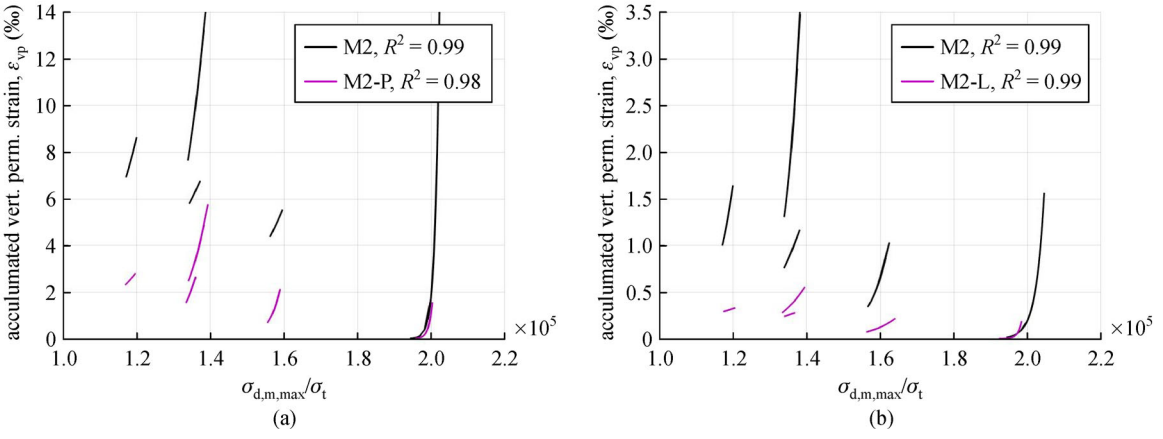

Fig. 14 Accumulated vertical permanent deformation, Shenton model: (a) P additive; (b) L additive.

Table 5 Values of a_{SH} and b_{SH} regression parameters for Shenton model

material	seq 1		seq 2		seq 3		seq 4		seq 5	
	a_{SH}	b_{SH}	a_{SH}	b_{SH}	a_{SH}	b_{SH}	a_{SH}	b_{SH}	a_{SH}	b_{SH}
M2 (w = 5%)	2.46E–54	1.79E2	3.13E–2	1.10E1	6.81E–1	7.24E0	1.69E0	8.90E0	4.89 E–2	1.73E1
M2-P	3.84E–65	2.14E2	6.10E–11	5.23E1	4.96E–4	2.78E1	6.48E–1	8.13E0	4.10E–3	2.18E1
M2 (w = 1%)	3.61E–29	9.20E1	5.02E–7	2.99E1	1.30E–2	1.38E1	4.07E–2	2.02E1	1.53E–4	3.09E1
M2-L	2.32E–59	1.94E2	3.36E–6	2.23E1	2.87E–2	7.23E0	1.34E–1	4.81E0	3.31E–3	1.53E1

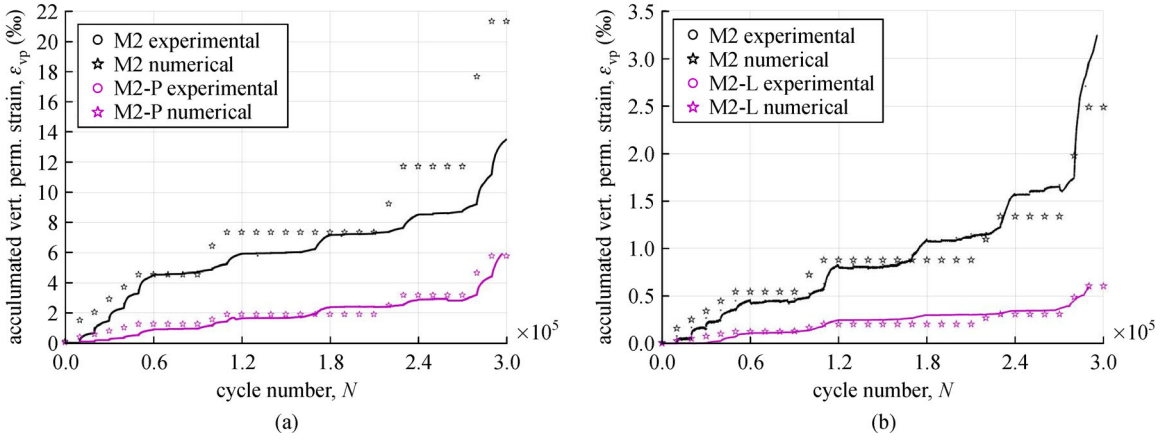

Fig. 15 Accumulated vertical permanent deformation, Tresca plasticity model: (a) P additive; (b) L additive.

P additive, whereas Fig. 16(b) displays the results for the L additive.

The Tresca plasticity criterion tends to overestimate the results, whereas the von Mises plasticity criterion tends to underestimate them. Table 6 reports the values of the plastic tangent modulus.

4 Conclusions

This study investigated the use of two stabilizing agents based on organosilane and lignosulfonate to enhance the mechanical performance of aggregates to be employed as construction materials in unbound courses of road pavements. The investigation was achieved by means of RLTTs.

The experimental data obtained were analyzed according to the models available in the literature regarding both the resilient modulus and accumulated vertical permanent deformation. A finite element model was developed to simulate the actual RLTT and compare the numerical and experimental results in terms of accumulated vertical

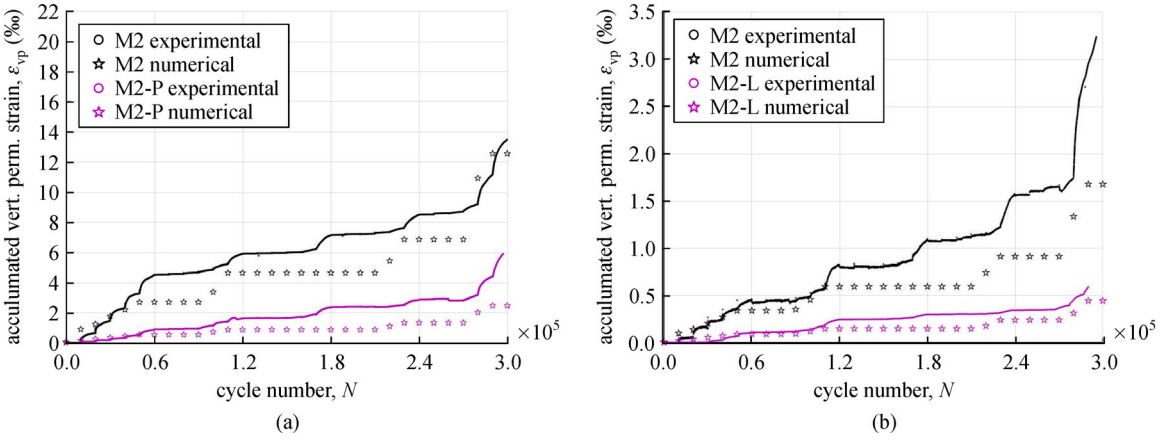

Fig. 16 Accumulated vertical permanent deformation, von Mises plasticity model: (a) P additive; (b) L additive.

Table 6 Plastic modulus values for Tresca and von Mises models

material	plastic modulus (kPa)	
	Tresca	von Mises
M2 (w = 5%)	11323	16984
M2-P	28370	42555
M2 (w = 1%)	42566	48566
M2-L	60153	62566

permanent deformation. Non-linear elastic and plastic constitutive relationships were implemented. The following conclusions can be drawn.

1) The outcomes of the RLTTs indicate that both the P and L agents remarkably improve the mechanical properties of the aggregates, and the enhancement includes both the resilient modulus and the development of permanent deformation.

2) The models used to interpret the experimental data referring to the resilient modulus (Hicks and Monismith, Uzan) and vertical permanent deformation (Coulomb, Barksdale, Sweere, Hyde, and Shenton) highlight that the investigated additives are effective technologies for enhancing the mechanical properties of crushed rocks.

3) In the finite element simulation of the RLTT, the Tresca plasticity model tends to overestimate the experimental results of permanent vertical deformation, whereas the von Mises plasticity model tends to underestimate them.

4) Both organosilane and lignosulfonate show promising results in stabilizing "weak" aggregates. The objective of future research could, for example, deal with accomplishing full-scale tests. Moreover, the finite element model can be expanded to the analysis of an actual road.

Acknowledgements The study was financed by the Norwegian Public Roads Administration (Grant No. 25134404. Sparks AS (Asker, Norway) and Zydex Industries (Vadodara, India) courteously provided the polymer-based additive. Borregaard AS (Sarpsborg, Norway) courteously provided the lignin-based additive. The authors do not have any conflicts of interest with other entities or researchers.

Notation

a: apparent attraction

a_{BA}: first regression parameter, Barksdale model

a_{HY}: regression parameter, Hyde model

a_{SH}: first regression parameter, Shenton model

a_{SW}: first regression parameter, Sweere model

b_{BA}: second regression parameter, Barksdale model

b_{SH}: second regression parameter, Shenton model

b_{SW}: second regression parameter, Sweere model

$k_{1,HM}$: first regression parameter, Hicks and Monismith model

$k_{1,UZ}$: first regression parameter, Uzan model

$k_{2,HM}$: second regression parameter, Hicks and Monismith model

$k_{2,UZ}$: second regression parameter, Uzan model

$k_{3,UZ}$: third regression parameter, Uzan model

Log: decimal logarithm

M_R: resilient modulus

N: number of load cycles

R^2: coefficient of determination for goodness of fit

w: gravimetric moisture content

$\dot{\varepsilon}$: strain rate

ε_{ve}: residual (or elastic or recoverable) vertical strain

ε_{vp}: permanent (or plastic or not recoverable) vertical strain

θ: bulk stress

θ_m: mean bulk stress

ρ: mobilized angle of friction

σ_1: major principal stress

σ_2: intermediate principal stress

σ_3: minor principal stress

σ_a: reference pressure

σ_d: deviatoric stress

$\sigma_{d,m}$: mean deviatoric stress

σ_t: triaxial (or confining) stress

σ_y: initial yield stress

τ_{oct}: octahedral shear stress

φ: angle of friction at the incremental failure

CEN: Comité Européen de Normalisation

LA: Los Angeles (test)

LVDT: Linear variable differential transducer

MDE: micro-Deval (test)

MS HSL: Multi-stage high stress level

MS LSL: Multi-stage low stress level

NPRA: Norwegian Public Roads Administration

OMC: Optimum moisture content

RLTT: Repeated load triaxial test

SS HSL: Single-stage high stress level

SS LSL: Single-stage low stress level

UGM: Unbound granular material

References

1. NPRA. The E39 Coastal Highway Route. Available at the website of 'The E39 Coastal Highway Route'. 2017
2. Dunham K K. Coastal Highway Route E39—Extreme crossings. Transportation Research Procedia, 2016, 14: 494–498
3. Gomes Correia A, Winter M G, Puppala A J. A review of sustainable approaches in transport infrastructure geotechnics. Transportation Geotechnics, 2016, 7: 21–28
4. Riviera P P, Bellopede R, Marini P, Bassani M. Performance-based re-use of tunnel muck as granular material for subgrade and sub-

base formation in road construction. Tunnelling and Underground Space Technology, 2014, 40: 160–173
5. Petkovic G. Recycling in Norwegian conditions. In: Bearing Capacity of Roads, Railways and Airfields—Proceedings of the 5th International Conference on the Bearing Capacity of Roads, Railways and Airfields. Trondheim: Tapir, 2005
6. Teknologirådet. Norwegian Board of Technology (NBT) | Norway 2030 Archive. Available at the website of Norway 2030. 2012
7. Barbieri D M, Hoff I, Mork H. Laboratory investigation on unbound materials used in a highway with premature damage. In: Bearing Capacity of Roads, Railways and Airfields—Proceedings of the 10th International Conference on the Bearing Capacity of Roads, Railways and Airfields. Trondheim: Tapir, 2017
8. NPRA. Norwegian Pavement Design Handbook N200. Version 2018. Oslo: Norwegian Public Roads Administration, 2018
9. NPRA. Norwegian Pavement Design Handbook N200. Version 2014. Oslo: Norwegian Public Roads Administration, 2014
10. CEN. Tests for Geometrical Properties of Aggregates. Part 1: Determination of Particle Size Distribution. Sieving Method. Brussels: European Committee for Standardization, 2012
11. CEN. Tests for Mechanical and Physical Properties of Aggregates. Part 3: Determination of Particle Shape—Flakiness Index. Brussels: European Committee for Standardization, 2012
12. CEN. Tests for Mechanical and Physical Properties of Aggregates. Part 2: Methods for the Determination of Resistance to Fragmentation. Brussels: European Committee for Standardization, 2010
13. CEN. Tests for Mechanical and Physical Properties of Aggregates. Part 1: Determination of the Resistance to Wear (Micro-Deval). Brussels: European Committee for Standardization, 2011
14. Liu J, Zhao S, Mullin A. Laboratory assessment of Alaska aggregates using Micro-Deval test. Frontiers of Structural and Civil Engineering, 2017, 11(1): 27–34
15. Barbieri D M, Hoff I, Mørk M B E. Mechanical assessment of crushed rocks derived from tunnelling operations. In: The 5th GeoChina International Conference 2018—Civil Infrastructures Confronting Severe Weathers and Climate Changes from Failure to Sustainability. Hangzhou: Springer, 2019, 225–241
16. Arulrajah A, Mohammadinia A, Horpibulsuk S, Samingthong W. Influence of class F fly ash and curing temperature on strength development of fly ash-recycled concrete aggregate blends. Construction & Building Materials, 2016, 127: 743–750
17. Behnood A. Soil and clay stabilization with calcium- and non-calcium-based additives: A state-of-the-art review of challenges, approaches and techniques. Transportation Geotechnics, 2018, 17: 14–32
18. Jiang Y J, Fan L F. An investigation of mechanical behavior of cement-stabilized crushed rock material using different compaction methods. Construction & Building Materials, 2013, 48: 508–515
19. Mohammadinia A, Arulrajah A, Haghighi H, Horpibulsuk S. Effect of lime stabilization on the mechanical and micro-scale properties of recycled demolition materials. Sustainable Cities and Society, 2017, 30: 58–65
20. Myre J. The Use of Cold Bitumen Stabilized Base Course Mixes in Norway. Oslo, 2014, 1–14
21. NPRA. Cold Bitumen Stabilized Base Layers. Oslo: Norwegian Public Roads Administration, 2014
22. Siripun K, Jitsangiam P, Nikraz H. Characterization analysis and design of hydrated cement treated crushed rock base as a road base material in Western Australia. International Journal of Pavement Research and Technology, 2010, 10: 39–47
23. Foroutan Mirhosseini A, Kavussi A, Tahami S A, Dessouky S. Characterizing temperature performance of bio-modified binders containing RAP binder. Journal of Materials in Civil Engineering, 2018, 30(8): 04018176
24. Barbieri D M, Mofid S A, Hoff I, Jelle B P. Nanoscale technology enhancement of crushed rocks' mechanical properties for pavement applications. In: The 6th International Symposium on Nanotechnology in Construction. Hong Kong, China, 2018
25. Huang Y, Wang L. Experimental studies on nanomaterials for soil improvement: A review. Environmental Earth Sciences, 2016, 75(6): 497–507
26. Paul D R, Robeson L M. Polymer nanotechnology: Nanocomposites. Polymer, 2008, 49(15): 3187–3204
27. Roco M C. Broader societal issues of nanotechnology. Journal of Nanoparticle Research, 2003, 5(3/4): 181–189
28. Sobolev K, Shah S P. Nanotechnology in construction. In: Proceedings of the 5th International Symposium on Nanotechnology in Construction NICOM5. Chicago: Springer, 2015: 509
29. Sobolev K. Modern developments related to nanotechnology and nanoengineering of concrete. Frontiers of Structural and Civil Engineering, 2016, 10(2): 131–141
30. Santoni R L, Tingle J S, Webster S L. Stabilization of silty sand with nontraditional additives. Transportation Research Record: Journal of the Transportation Research Board, 2002, 1787(1): 61–70
31. Alazigha D P, Indraratna B, Vinod J S, Heitor A. Mechanisms of stabilization of expansive soil with lignosulfonate admixture. Transportation Geotechnics, 2018, 14: 81–92
32. Barbieri D M, Hoff I, Mørk M B E. Innovative stabilization techniques for weak crushed rocks used in road unbound layers: A laboratory investigation. Transportation Geotechnics, 2019, 18: 132–141
33. Ghadimi B, Nikraz H. A comparison of implementation of linear and nonlinear constitutive models in numerical analysis of layered flexible pavement. Road Materials and Pavement Design, 2017, 18(3): 550–572
34. Sun W, Wang L, Wang Y. Mechanical properties of rock materials with related to mineralogical characteristics and grain size through experimental investigation: A comprehensive review. Frontiers of Structural and Civil Engineering, 2017, 11(3): 322–328
35. Lekarp F, Isacsson U, Dawson A. State of the art. I: Resilient response of unbound aggregates. Journal of Transportation Engineering, 2000, 126(1): 66–75
36. Lekarp F, Isacsson U, Dawson A. State of the art. II: Permanent strain response of unbound aggregates. Journal of Transportation Engineering, 2000, 126(1): 76–83
37. Uthus L, Tutumluer E, Horvli I, Hoff I.Influence of grain shape and texture on the deformation properties of unbound aggregates in pavements. International Journal of Pavements, 2007, 6: 75–87
38. CEN. Unbound and Hydraulically Bound Mixtures. Part 4: Test Methods for Laboratory Reference Density and Water Content. Vibrating hammer. Brussels: European Committee for Standardization, 2003

39. CEN. Cyclic Load Triaxial Test for Unbound Mixture. Brussels: European Committee for Standardization, 2004
40. Erlingsson S, Rahman M S, Salour F. Characteristic of unbound granular materials and subgrades based on multi stage RLT testing. Transportation Geotechnics, 2017, 13: 28–42
41. Hoff I, Arvidsson H, Erlingson S, Houben L J M, Kolisoja P, Schwartz C W. Round robin investigation on the cyclic triaxial test for unbound granular materials. In: Bearing Capacity of Roads, Railways and Airfields-Proceedings of the 7th International Conference on the Bearing Capacity of Roads, Railways and Airfields, BCRRA 2005. Trondheim: Tapir, 2005
42. Zhalehjoo N, Tolooiyan A, Mackay R, Bodin D. The effect of instrumentation on the determination of the resilient modulus of unbound granular materials using advanced repeated load triaxial testing. Transportation Geotechnics, 2018, 14: 190–201
43. Hicks R G, Monismith C L. Factors influencing the resilient properties of granular materials. Highway Research Record, 1971, 345: 15–31
44. Uzan J. Characterization of granular material. Transportation Research Record: Journal of the Transportation Research Board, 1985: 52–59
45. Uzan J, Witczak M W. The Universal Airport Pavement Design System, Report I of IV: Granular Material Characterization. 1988
46. Werkmeister S, Dawson A R, Wellner F. Pavement design model for unbound granular materials. Journal of Transportation Engineering, 2004, 130(5): 665–674
47. Werkmeister S, Dawson A, Wellner F. Permanent deformation behavior of granular materials and the shakedown concept. Transportation Research Record: Journal of the Transportation Research Board, 2005, 1757: 75–81
48. Gidel G, Hornych P, Chauvin J J, Breysse D, Denis A. A new approach for investigating the permanent deformation behaviour of unbound granular material using the repeated load triaxial apparatus. Bulletin Des Laboratories Des Pont Chaussees, 2001, 233: 5–21
49. Hoff I, Bakløkk L J, Aurstad J. Influence of laboratory compaction method on unbound granular materials. In: The 6th International Symposium on Pavements Unbound. Nottingham: CRC Press, 2003
50. Barksdale R D. Laboratory evaluation of rutting in basecourse materials. In: The 3rd Conference on the Structural Design of Asphalt Pavements. London: Cushing-Malloy, 1972, 161–174
51. Sweere G T H. Unbound Granular Bases for Roads. Delft: University of Delft, 1990
52. Erlingsson S, Rahman M S. Evaluation of permanent deformation characteristics of unbound granular materials by means of multi-stage repeated-load triaxial tests. Transportation Research Record: Journal of the Transportation Research Board, 2013, 2369(1): 11–19
53. Rahman M S, Erlingsson S. Predicting permanent deformation behaviour of unbound granular materials. International Journal of Pavement Engineering, 2015, 16(7): 587–601
54. Hyde A F L. Repeated Load Triaxial Testing of Soils. London: University of Nottingham, 1974
55. Shenton M J. Deformation of railway ballast under repeated loading. In: Symposium on Railroad Track Mechanics. New Jersey: Princeton University, 1975
56. COMSOL. COMSOL Multiphysics 5.3 Reference Manual. Burlington: COMSOL Inc., 2017
57. Kim M, Tutumluer E, Kwon J. Nonlinear pavement foundation modeling for three-dimensional finite-element analysis of flexible pavements. International Journal of Geomechanics, 2009, 9(5): 195–208
58. Hornych P, Chazallon C, Allou F, El Abd A. Prediction of permanent deformations of unbound granular materials in low traffic pavements. Road Materials and Pavement Design, 2007, 8(4): 643–666
59. Chazallon C, Hornych P, Mouhoubi S. Elastoplastic model for the long-term behavior modeling of unbound granular materials in flexible pavements. International Journal of Geomechanics, 2006, 6(4): 279–289
60. David C T, García-Rojo R, Herrmann H J, Luding S. Hysteresis and creep in powders and grains. Powders Grains, 2005, 2005: 291–294